5474–5488 *Nucleic Acids Research, 2011, Vol. 39, No. 13* *Published online 18 March 2011*
doi:10.1093/nar/gkr149

Irreparable complex DNA double-strand breaks induce chromosome breakage in organotypic three-dimensional human lung epithelial cell culture

Aroumougame Asaithamby[1,*], Burong Hu[2], Oliver Delgado[3], Liang-Hao Ding[1], Michael D. Story[1], John D. Minna[4], Jerry W. Shay[3] and David J. Chen[1,*]

[1]Division of Molecular Radiation Biology, Department of Radiation Oncology, University of Texas, Southwestern Medical Centre, Dallas, TX 75390, USA, [2]Key Laboratory of Heavy Ion Radiation Biology and Medicine, Institute of Modern Physics, Chinese Academy of Sciences, Lanzhou 730000, P. R. of China, [3]Department of Cell Biology and [4]The Hamon Center for Therapeutic Oncology, Department of Internal Medicine and Pharmacology, The University of Texas Southwestern Medical Center at Dallas, Dallas, TX 75390, USA

Received January 12, 2011; Revised February 25, 2011; Accepted February 28, 2011

ABSTRACT

DNA damage and consequent mutations initiate the multistep carcinogenic process. Differentiated cells have a reduced capacity to repair DNA lesions, but the biological impact of unrepaired DNA lesions in differentiated lung epithelial cells is unclear. Here, we used a novel organotypic human lung three-dimensional (3D) model to investigate the biological significance of unrepaired DNA lesions in differentiated lung epithelial cells. We showed, consistent with existing notions that the kinetics of loss of simple double-strand breaks (DSBs) were significantly reduced in organotypic 3D culture compared to kinetics of repair in two-dimensional (2D) culture. Strikingly, we found that, unlike simple DSBs, a majority of complex DNA lesions were irreparable in organotypic 3D culture. Levels of expression of multiple DNA damage repair pathway genes were significantly reduced in the organotypic 3D culture compared with those in 2D culture providing molecular evidence for the defective DNA damage repair in organotypic culture. Further, when differentiated cells with unrepaired DNA lesions re-entered the cell cycle, they manifested a spectrum of gross-chromosomal aberrations in mitosis. Our data suggest that downregulation of multiple DNA repair pathway genes in differentiated cells renders them vulnerable to DSBs, promoting genome instability that may lead to carcinogenesis.

INTRODUCTION

DNA damage and consequent mutations initiate the multistep carcinogenic process. Among the many radiation-induced lesions, DNA double-strand breaks (DSBs) are considered the key precursors of most early and late effects of radiation. There are qualitative differences between the low-linear energy transfer (LET) and high- [i.e. high charge and energy (HZE)] LET radiation both in induction and in repair of DNA damage (1–3). Isolated DNA lesions (mainly induced by low-LET radiation), including DSBs, single-strand breaks (SSBs) and damaged bases, are generally repaired efficiently. In contrast, due to the unique pattern of energy deposition produced by HZE particle traversal, DNA damage induced by high-LET radiation is skewed toward multiple damaged sites (MDS) or complex DNA lesions. Complex DNA damages are a unique class of DNA lesions that include two or more individual lesions within one or two helical turns of the DNA (4). The lesions within the clustered damage sites can be abasic sites (also known as apurinic/apyrimidinic sites or APs), damaged bases (oxidized purines or pyrimidines), SSBs or DSBs (5–7). Convincing evidence indicates that complex lesions are more difficult to repair than isolated lesions and are, in some instances, irreparable; this has been associated with the increased relative biological effectiveness of death, chromosomal aberrations, mutagenesis and carcinogenesis in high-LET irradiated cells compared to those treated with low-LET radiation (4,8,9).

Most of the work on induction and repair of DNA damage and signaling pathways involved in DNA repair and carcinogenesis has been performed in proliferating, two-dimensional (2D) culture systems. Although these

*To whom correspondence should be addressed. Tel: +214 648 5597; Fax: +214 648 5995; Email: David.Chen@UTsouthwestern.edu
Correspondence may also be addressed to Aroumougame Asaithamby. Tel: +214 648 1249; Fax: +214 648 5995;
Email: Aroumougame.Asaithamby@UTsouthwestern.edu

systems are useful, results are difficult, if not impossible, to confirm *in vivo*. When grown in 2D, cells do not recapitulate the structural organization or functional differentiation of the cells *in viv*o. Cells *in vivo* interact with their environment in three-dimensions, contacting neighboring cells, the extracellular matrix and soluble chemicals and are subject to mechanical forces. Three-dimensional (3D) extracellular matrix (ECM) provides structural support and cues (received via transmembrane receptors) that direct cytoskeletal and chromatin organization to maintain tissue integrity (10). Although 2D cells can respond to the mechanical nature of the culture system, they have little capacity to manipulate the composition and mechanical properties of the ECM itself (11). The phenotypes of cells cultured in 3D matrices are altered compared to those grown in 2D; proliferation is inhibited and their ability to form higher order structures is enhanced (12). The 3D culture systems are thus more biologically relevant models for investigation of functions of genes and pathways than are 2D systems (10).

The DNA damage response of proliferating cells is different from that of differentiated cells. Many groups have studied DNA repair in differentiated cells; the often divergent results may be due to unique properties of distinct classes of differentiated cells. The general notion is that terminally differentiated cells never replicate their genomes, hence, their need to repair DNA damage is reduced (13). Although DNA damage from oxidative metabolism and exogenous agents may be similar in dividing and non-dividing cells, in cells that have stopped dividing, damaged chromatin is not a threat as there will be no progeny cells. Yet, differentiated cells are transcriptionally active and retain the need to preserve the integrity of the transcribed genome throughout the life span. For some long-lived and essentially irreplaceable cells such as neurons, DNA repair may be more essential than for short-lived cells, such as terminally differentiated blood cells (13).

Proliferating cells handle the risk of creating DSBs during DNA replication by expressing and activating the homologous recombination repair machinery in a cell cycle-dependent fashion only during S-phase (14). Moreover, during cell division, DNA damage checkpoint proteins survey for unrepaired DNA damage to prevent cell-cycle progression at G1-S and G2-M, thereby preventing the spread of mutations to progeny. As a consequence of their reduced need for DNA repair, non-dividing cells have an attenuated DSB response (13,15). However, in certain circumstances, such as when tissue must be repaired, these cells can re-enter the cell cycle and DNA damage might initiate the multistep carcinogenic process.

Although differentiated cells have a reduced capacity to repair DNA lesions, the biological impact of unrepaired DNA DSBs in differentiated lung epithelial cells is unclear. Here, we established a novel 3D organotypic human lung model by culturing human bronchial epithelial cells in reconstituted basement membrane (Matrigel) on top of human fetal lung fibroblasts. This system allowed us to investigate the biological significance of defective DSBs repair in differentiated cells. Using this organotypic 3D model in combination with a newly established cytological imaging approach, we found that the kinetics of DNA DSBs repair was substantially compromised in differentiated cells compared to kinetics in 2D culture. In contrast to proliferating cells, cells in 3D organotypic culture expressed reduced levels of multiple DNA damage repair pathway genes, providing molecular evidence for the reduced capacity of DNA lesions repair in differentiated cells. Significantly, the unrepaired DNA DSBs in organotypic culture resulted in the formation of a spectrum of gross-chromosomal aberrations when cells re-entered the cell cycle. Thus, downregulation of multiple DNA repair pathway genes in differentiated cells renders them vulnerable to complex DSBs that might promote genome instability leading to carcinogenesis.

MATERIALS AND METHODS

Monolayer cell culture

Human bronchial epithelial cells (HBECs) immortalized with human telomerase reverse transcriptase (hTERT) were maintained at 37°C in a humidified 5% CO_2 incubator as described previously (16). To generate the HBEC-EGFP 53BP1 stable line, HBECs were transfected with linearized EGFP-53BP1 mammalian expression plasmid (pcDNA, Invitrogen) using Nucleofector (Amaxa). The cells were selected with 20 μg/ml hygromycin for 10 days. Stable lines were maintained as described previously (17).

3D organotypic culture

Construction of 3D organotypic HBEC cultures was performed as described previously (18) with the following modifications: HBECs were suspended in Bronchiole Epithelial Basal Medium (BEBM, Lonza) and DMEM high glucose with L-glutamine and sodium pyruvate (Hyclone) at a 1:1 ratio. The medium was supplemented with 5 μg/ml bovine pituitary extract, 0.05 μM hydrocortisone, 0.5 ng/ml hEGF, 1.35 μM epinephrine, 0.46 μM insulin, 5 nM triiodothyronine, 62.5 nM transferrin, 25 nM retinoic acid and 1 mM calcium chloride. Cell suspensions (20 μl) at a density of 1.5 million cells/ml were resuspended in 250 μl pre-thawed Growth Factor Reduced Phenol-Red Free Matrigel (BD Biosciences) and seeded into single, 24-mm diameter Transwell® permeable inserts with 0.4 μm pore size (Corning, Lowell, MA, USA). Matrigel cultures in the Transwell® permeable inserts were allowed to gel for 30 min at 37°C and then 200 μl BEBM:DMEM media with supplements was added. One hundred thousand IMR90 human lung fibroblasts in 500 μl BEBM:DMEM media with supplements were pre-seeded into single wells of a 12-well tissue culture plate (BD Falcon) 48 h prior to the experiment. Matrigel cultures in Transwell® permeable inserts were then placed on top of the IMR 90 cultures to receive growth stimulus. Cultures were grown at 37°C for 5 days with media changed every 2 days. After 5 days, Matrigel cultures were separated from the IMR90 coculture and were maintained at 37°C for ~9 days. For branching analysis, cultures were maintained at 37°C for an additional

15 days with IMR90 coculture to provide growth as well as differentiation stimuli.

Irradiation

For low-LET γ-irradiation, a ^{137}Cs γ-rays source was used. For doses ~25 cGy, attenuators were placed between the source and the samples to result in a dose rate of ~4 cGy/min; for higher doses, no attenuators were used and the dose rate was ~3.5 Gy/min. High-LET iron (Fe) particles beams were generated at the NASA Space Radiation Laboratory at Brookhaven National Laboratory. The energy of the Fe particles used was 1 GeV/n and the dose rate ranged from 50 to 100 cGy/min. The LET of the Fe was 150 keV/μm. The residual ranges of the beams were determined before each experiment and were used to calculate the track-averaged LET values.

Immunostaining

For 2D cultures, immunostaining was carried out as described previously (17). Briefly, cells were seeded at 2×10^4 cells in each well of a four-well chamber slide, cultured for 48 h prior to irradiation and then incubated (37°C, 5% CO_2) for various times. The irradiated cells were fixed with 4% PFA for 20 min at room temperature and permeabilized with 0.5% Triton X-100 in PBS while on ice for 10 min. Non-specific binding sites were blocked with 5% goat serum in PBS for 60 min at room temperature prior to probing with primary antibodies. Anti-pT2609 monoclonal antibody was generated as described previously (19). Anti-γH2AX mouse monoclonal (U.S. Biologicals), 53BP1 and anti-pT68-Chk2 rabbit polyclonal (Cell Signaling), anti-Ki-67 rabbit monoclonal (Abcam), anti-E-Cadherin Rat monoclonal (Abcam), anti-surfactant protein A mouse monoclonal (Abcam), anti-α-actin mouse monoclonal (Sigma) antibodies were used. Secondary antibodies (anti-mouse or rat or rabbit conjugated with Alexa 488/633 or Rhodamine) were purchased from Molecular Probes. The 3D structures in Matrigel were immunostained as described previously (18) with the following modifications: the 3D cultures were fixed with 4% PFA for 30 min at room temperature and thereafter washed three times with PBS (20 min each). Cells were washed three times with 100 mM glycine in PBS for 20 min each at room temperature and then permeabilized with 0.5% Triton X-100 in PBS for 12 min on ice. Primary blocking was done by incubating the structures in immunofluorescence (IF) buffer (0.1% BSA/0.2% Triton X-100/0.05% Tween-20/5% goat serum in PBS) for 4 h and secondary blocking was performed by incubating in IF buffer with 5% goat serum and 20 μg/ml goat anti-mouse F(ab')$_2$ fragment (Jackson Laboratories) for an additional 4 h. The 3D structures were incubated in the primary antibody diluted in 5% goat serum/1× PBS overnight at 24°C. After incubation, the structures were washed three times with 1% BSA in PBS, 30 min each and then incubated with the appropriate Alexa Fluor secondary antibodies diluted in 1% BSA and 2.5% goat serum for 1 h. The structures were washed five times with 1% BSA for 20 min each. The nuclei were counterstained with DAPI (Vector shield).

Image acquisition

Images of 3D structures were captured using an LSM 510 Meta laser scanning confocal microscope with a ×63 1.4 NA Plan-Apochromat oil immersion objective. Images were taken at z-sections (120–180 sections) of 0.5 μm intervals using the 488-nm (EGFP-53BP1), 543-nm (Rhodamine), 633-nm (Alexa 633) and 405-nm (for DAPI) lasers. The tube current of the 488-nm argon laser was set at 6.1 A. The laser power was typically set to 5–10% transmission with the pinhole opened to 1–3 Airy units. Images of 2D cultures were acquired as described (17).

Foci dissolution kinetics assay

The z-sections of 15–20 and 120–180 for 2D cultures and 3D structures, respectively, were assembled using Imaris software (Bitplane) and then used for further analysis. For counting 53BP1 foci, we utilized the spot detection function of the Imaris software (17). In this spot-detection algorithm, the spatial position along the *x*-, *y*- and *z*-axes and the intensity of the EGFP-53BP1 focus the spot represents were determined. We confirmed the accuracy of foci counting using colocalization function of the same software where we observed >99% colocalization of the detected spots with EGFP-53BP1 foci. Quantification of foci was done from images of 100–250 cells for 2D cells and 15–20 3D structures for each dose and time point from at least three independent experiments. The average focus number per nucleus of mock-irradiated cells was subtracted from the average focus number per nucleus of each time or dose. A non-linear regression analysis and curve fitting were used to assess the focus dissolution kinetics (Sigma Plot, Version 11.0).

Conversion of 3D structures to monolayers

3D structures were recovered from Matrigel using recovery solution (BD Biosciences) according to the manufacturer's instructions with minor modifications. Briefly, 3D cultures were first washed with ice-cold PBS, then with ice-cold recovery solution and removed from the transwells using a sterile scalpel. The Matrigel containing the 3D structures was removed from the membrane, transferred to a pre-chilled 15 ml tube containing the recovery solution (1 ml per transwell), incubated on ice for 45–60 min with intermittent mixing and then centrifuged at 1000 rpm for 10 min at 4°C. The supernatant containing the dissolved Matrigel was discarded and the 3D structures were washed once with PBS. To make single-cell suspensions of recovered 3D structures, cells were trypsinized using trypsin-EDTA (0.25%, Invitrogen). Cells were then either fixed with 70% ice-cold ethanol for flow cytometry or maintained at 37°C in a humidified 5% CO_2 incubator for chromosome analysis.

BrdU labeling

Cells were labeled with BrdU in HBEC growth medium. For 2D culture, cells were pulsed with 30 μM BrdU for 30 min. For 3D culture, cells were pulsed with 100 μM BrdU for 1 h at 37°C. Subsequently, cells were washed twice with PBS. For flow cytometry, 3D structures were dissociated from the Matrigel and fixed with ice-cold 70% ethanol. For immunostaining, 2D and 3D cultures were fixed with 4% PFA.

Flow cytometry

The 3D structures were dispersed into single-cell suspensions by treatment with 0.25% trypsin (Invitrogen) at 37°C for 10 min. Cells were washed twice in PBS and fixed with ice-cold 70% ethanol at −20°C overnight. For BrdU immunostaining, cells were first washed twice with cold PBS and then treated with 100 μg/ml RNase/5% Tween-20 in PBS at 37°C for 30 min. To denature DNA double strands to single strands, cells were resuspended in 3–4 M HCl (1 ml per 10^6 cells) containing 0.5% Tween-20 and incubated at 37°C for 30 min and then neutralized by washing twice with PBS. Following neutralization, cells were incubated in 100 μl PBS containing 0.1% Tween-20, 1% BSA and anti-BrdU antibody conjugated with Alexa 488 (1:100, Molecular probes) at room temperature for 2 h. After washing with 1% BSA, cells were stained with 10 μg/ml propidium iodide (Sigma) at room temperature for 30 min and subjected to flow cytometry (FACScan, Becton Dickinson). For immunostaining of cells with Ki-67, cells were permeabilized in Triton X-100 (0.25%, Sigma) on ice for 5 min, incubated in blocking solution (5% goat serum in PBS) at room temperature for 30–60 min and then incubated with primary antibodies (1:200–300, in 5% goat serum) at room temperature for another 2 h. Subsequently, cells were washed with 1% BSA in PBS and incubated with appropriate secondary antibodies (1:400–800, in 2.5% goat serum, 1% BSA and PBS) at room temperature for 30 min, washed twice with 1% BSA and subjected to flow cytometry; the data were analyzed with CellQuest software (Becton Dickinson).

RNA purification, labeling and microarray hybridizations

Three independent samples from mock-irradiated 2D and 3D HBECs cultures were prepared as biological replicates for gene expression analysis. Total RNA from 2D and 3D cultures were extracted using Qiagen RNeasy Mini kit. RNA samples were amplified and labeled using Illumina Total Prep RNA amplification kit according to manufacturer's instruction. After amplification, the cRNA was checked for size and yield using the Bio-Rad Experion system. A total of 1.5 μg of cRNA was hybridized to an Illumina HumanWG-6 V3 Expression Bead Chip (Illumina, Inc.) using standard Illumina protocols with streptavidin-Cy3 (Amersham, Piscataway, NJ, USA) being used for detection. The slides were scanned on an Illumina Beadstation.

Data Analysis for gene expression and Microarray data accession number

Signal intensities of microarrays were summarized using BeadStudio v3.3 (Illumina, Inc). Background subtraction and quantile normalization were performed using model-based background correction for BeadArrays algorithm (20). Multidimentional scaling, clustering and two-sample *t*-test with multitesting corrections were performed using Partek Genomic Suit software. The cutoff for significantly changed genes were false discovery rate (FDR) < 0.01. Gene category enrichment analysis was performed using Ingenuity Pathway Analysis (20). The significant level for enrichment analysis was FDR < 0.05. The accession number for the newly reported microarray data is NCBI GEO series accession number GSE27520.

Cytogenetic analysis

The 3D structures were dissociated from the Matrigel 24 h following ionizing radiation (IR) and then cultured for an additional 24 h. Subsequently, chromosome preparations were made by accumulating metaphases in the presence of 0.1 μg/ml colcemid (Irvine Scientific) for 8 h and collected by trypsinization. Cells were then washed twice with PBS and incubated in 10 ml of hypotonic solution (0.075 M KCl) at 37°C for 15 min. Cells were pre-fixed with 1/10 volume of ice-cold methanol:acetic acid (3:1 ratio) in hypotonic solution and then centrifuged at 1000 RPM for 5 min at 4°C. Subsequently, the cells were fixed with methanol:acetic acid (3:1 ratio) on ice for 30 min and then with same fixative at −20°C until use. Cells were dropped onto pre-cleaned cover glass and stained with Giemsa stain (5%, KaryoMAX, GIBCO) for 5 min at room temperature and then washed with dH_2O. Images were taken using an Olympus microscope (×100 objective) equipped with an Image Spot camera (Spot Imaging Solutions).

Statistical analysis

For the analysis of DSB repair kinetics, the EGFP-53BP1 foci numbers obtained from 0.5, 1, 2, 4, 8, 12, 24, 48 and 72 h after irradiation were used. Foci numbers were fitted assuming two exponential components of rejoining according to the equation $y = Ae{-}bx + Ce{-}dx$ (21,22). The first term in the equation was fitted to the slow component of rejoining and the second term was fitted to the fast component of rejoining. Fitting was achieved using the double four parameters best fit equation, $y = A^*\exp(-b^*x) + C^*\exp(-d^*x)$ of Sigma Plot (version 11.0). Parameters A and C describe the amplitudes and parameters b and d are the rate constants of the slow and the fast components of rejoining, respectively. From these parameters, the fraction of DSBs rejoined by fast kinetics was calculated as $F_{\text{fast}} = A/A + C$ and slow kinetics was calculated as $F_{\text{slow}} = C/A + C$. The Student's *t*-test was performed to calculate the level of significance and a value of $P < 0.05$ was considered statistically significant.

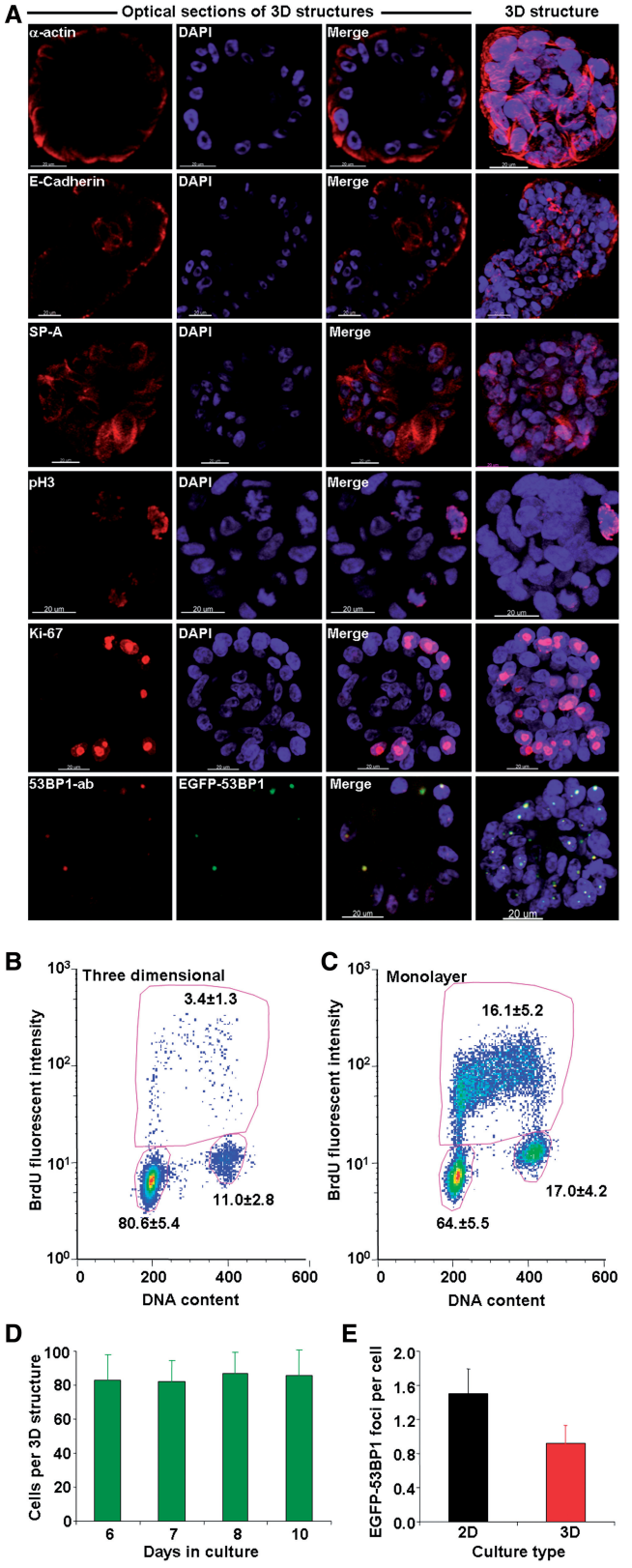

Figure 1. A novel human lung three-dimensional culture model for the study of differentiated cells response to DSBs. (**A**) Human bronchial epithelial cells (HBECs) form well-organized, growth-arrested structures when cultured in extracellular matrix and on top of IMR90 human lung fibroblasts. Representative optical sections and deconvoluted confocal microscopic images of 3D structures are shown. HBECs stably expressing EGFP-53BP1 grown in Matrigel for 6 days were immunostained with antibodies to α-actin, E-cadherin, SP-A, pH3, Ki-67 and 53BP1. The images were acquired using confocal microscopy and deconvoluted using Imaris software. (**B** and **C**) HBECs grown in 3D culture have fewer S-phase and more G1-phase cells than in 2D culture. Flow cytometric profiles of the cell cycle distribution of (B) 3D and (C) 2D cultures at the time of irradiation. HBECs in 2D and 3D cultures were pulse labeled with BrdU and then subjected to immunostaining and 'Flow cytometry' as described in 'Materials and Methods' section. Data are representative of at least three independent experiments. (**D**) Number of cells in 3D structures did not increase between 6 and 10 days in Matrigel culture. Images of 3D structures were acquired at Days 6, 7, 8 and 10 using confocal microscopy. The number of cells per 3D structure was counted using Imaris software. Cells in more than 100 3D structures were counted each day. (**E**) Cells in 3D structures have fewer spontaneous EGFP-53BP1 foci than cells in 2D culture. HBECs stably expressing EGFP-53BP1 grown in 2D and 3D cultures were immunostained with antibodies to 53BP1. The images were acquired using confocal microscopy and deconvoluted using Imaris software. More than 1000 2D cells and 100 3D structures were evaluated; error bars represent standard deviations calculated from three independent experiments.

RESULTS

A novel, organotypic, 3D, human lung epithelial cell culture model to study the responses of differentiated cells to DNA DSBs

To investigate the biological significance of unrepaired DSBs in differentiated cells, we have established a 3D human lung epithelial cell model by culturing human bronchial epithelial cells (HBECs) that stably express EGFP-53BP1 (17) in reconstituted basement membrane (Matrigel) on top of IMR90 fetal lung fibroblasts (Figure 1 and Supplementary Figure S1). After 6 days in Matrigel culture, the epithelial cells formed an acinus-like structure and a majority of these structures were hollow and characterized by E-cadherin-positive adherens junctions (Figure 1A). The cells were also positive for surfactant protein A (SP-A, Figure 1A), a protein associated with differentiation of alveolar type II cells during the saccular–alveolar stage of lung development (23). Immunostaining for phospho-histone 3 (pH3), a marker of mitosis (Figure 1A), indicated that the 3D structures consisted of very few M-phase cells. Pulse labeling with BrdU followed by flow cytometry analysis showed that ~85% of the cells in 3D structures were in G0/G1-phase, only 4% of cells were in S-phase (BrdU positive) and the remaining 11% of the cells were in G2/M-phase (Figure 1B). In monolayer (2D) cultures at Day 6, 64, 16 and 17% of cells were in G0/G1-, S- and G2/M-phases, respectively (Figure 1C). Cell proliferation-associated nuclear antigen Ki-67 is expressed in G1- (cells after mitosis), S-, G2- and M-phase cells and is absent in G0-phase cells, such as in quiescent and differentiated cells (24). Whereas ~99% of the HBECs in 2D cultures were positive for Ki-67, only 20% of the cells in 3D structures were positive for Ki-67 (Supplementary Figure S1A). This indicated that a majority (>80%) of the cells in the 3D culture were differentiated. After Day 6, no pH3 or BrdU positive cells were observed and the number of cells in 3D structures did not increase (Figure 1D), strongly suggesting that the model system had reached a growth arrested, differentiated state at Day

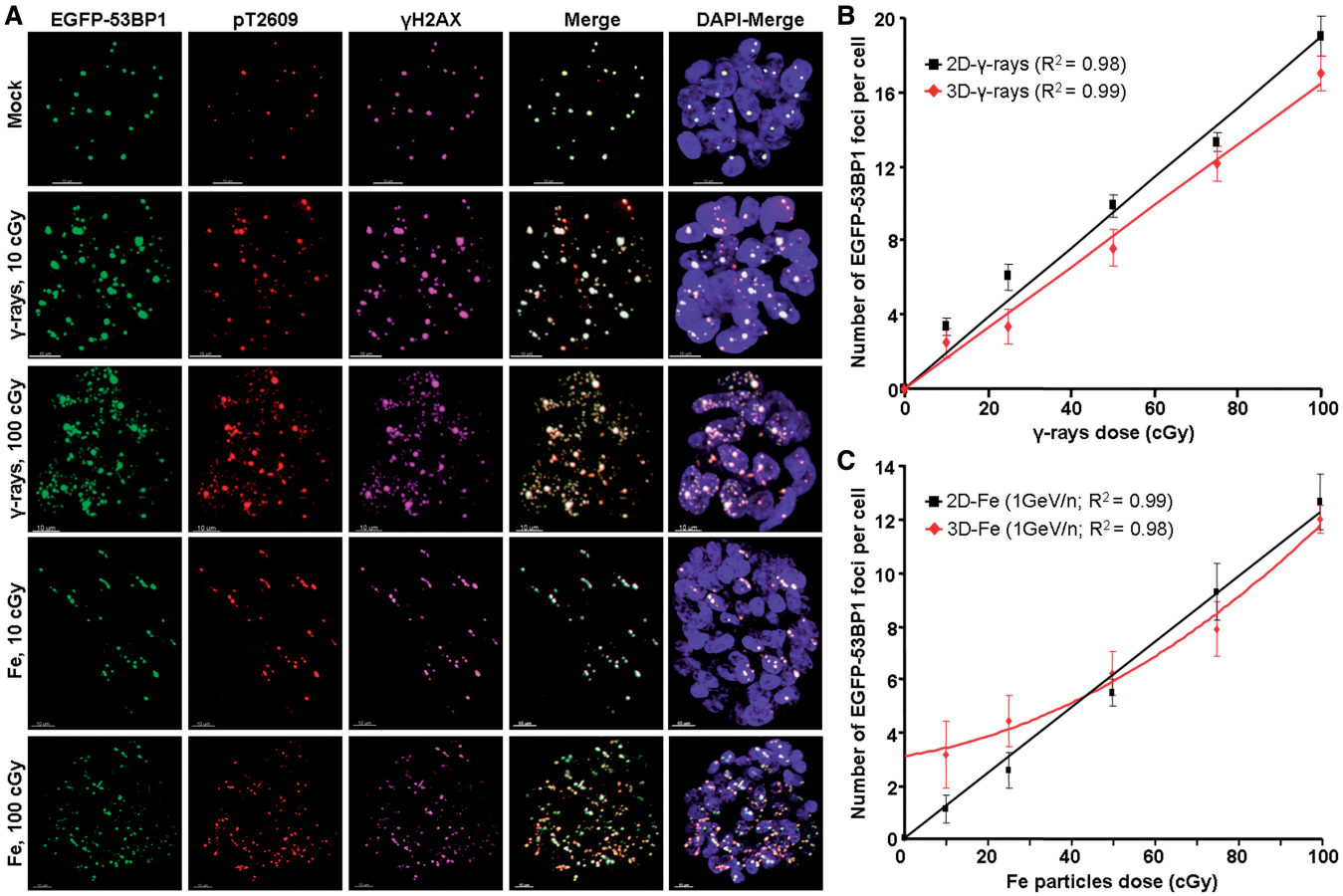

Figure 2. Number of DNA DSBs formed in 3D structures is dose- and LET-dependent. (**A**) Representative deconvoluted images of 3D structures showing co-localization of EGFP-53BP1 with γH2AX and DNA-PKcs (pT2609) after exposure of cells to graded doses of γ-rays and Fe particles. HBECs stably expressing EGFP-53BP1, grown in Matrigel for 6 days, were irradiated with indicated doses of γ-rays and Fe particles and were fixed at 30 min after irradiation. Subsequently, cells were immunostained with anti-γH2AX and DNA-PKcs (pT2609) antibodies and images were recorded using confocal microscopy. (**B**) Graph showing the number of EGFP-53BP1 foci formed at 30 min after exposure of 2D and 3D cultures to 10–100 cGy of γ-irradiation. (**C**) Graph showing the number of EGFP-53BP1 foci formed at 30 min after exposure of 2D and 3D cultures to 10–100 cGy of Fe particles irradiation. HBECs stably expressing EGFP-53BP1 grown in 2D and 3D cultures were irradiated with indicated doses of γ-rays and Fe particles and were fixed at 30 min after irradiation. The images were acquired using confocal microscopy and the foci numbers were counted using spot-detection function of Imaris software. The EGFP-53BP1 foci numbers in 200–400 cells from 2D culture and 15–18 3D structures were counted for each dose. The error bars represent standard deviations calculated from three independent experiments.

6 as previously reported for 3D cultures of immortalized HBECs (25). When grown in Matrigel for 15 days, HBECs exhibited branching morphogenesis (Supplementary Figure S1B). These results confirm that HBECs in Matrigel differentiate into tissue-specific structures; in this case the structures mimic those found in the peripheral lung.

A novel imaging approach reveals that the number of DSBs generated in cells in organotypic culture is dose- and LET-dependent

To directly visualize induction and repair of DSBs in organotypic culture, we first established a novel method for 3D imaging quantification of ionizing radiation-induced foci. The key advantage of this approach is its ability to directly visualize and measure DSBs in the organotypic 3D culture without any immunostaining. To accurately quantify the induction and repair of DSBs, we first evaluated the background levels of EGFP-53BP1 foci in 2D and 3D cultures. Examination of high-resolution deconvoluted images for 53BP1 foci revealed that there were, on average, two EGFP-53BP1 foci per cell in 2D culture at Day 6, whereas, there was on average, only one per cell in 3D structures (Figure 1E). Similar to previous findings (17), these foci were clearly colocalized with anti-53BP1 antibody stained 53BP1 (Figure 1A, bottom). We then verified that EGFP-53BP1 foci represent sites of DSBs by immunostaining with antibodies to phosphorylated DNA-PKcs (pT2609) and H2AX (γH2AX). After γ- or Fe particles irradiation, EGFP-53BP1 foci colocalized with DNA-PKcs and γH2AX foci in 3D (Figure 2A) and 2D cultures (Supplementary Figure S2), confirming that the EGFP-53BP1 foci mark the sites of DSBs and can be used as a surrogate marker to evaluate the kinetics of DNA DSBs repair in organotypic culture (26).

At 30 min after IR, we determined the number of EGFP-53BP1 foci over a range of doses from 10 to 100

cGy of γ- or Fe particles irradiation. The relationship between the number of foci induced per cell and the γ-rays dose delivered was linear for both 2D and 3D cultures (Figure 2B). The observed value of approximately 20 foci/Gy in 2D culture correlated with our previous 53BP1 foci measurements and with previous studies that showed 20–40 DSBs/Gy of γ-irradiation (17,27). In contrast to γ-irradiation, the relationship between the number of foci induced per cell and the Fe particles dose delivered was not linear in 3D structures (Figure 2C). Notably, the number of EGFP-53BP1 foci after 10 and 25 cGy of Fe particles irradiation was higher in 3D structures than in 2D culture. This could be due to the bystander effect. Thus, these results provide evidence that the relationship between the number of DSBs and the dose of Fe particles is dependent on the nature of cell culture model.

DNA DSBs are repaired with slower kinetics in organotypic 3D cultures

We investigated the dynamic loss of EGFP-53BP1 foci in 3D culture after 1 Gy of low-LET (γ-rays) or high-LET (Fe particles) IR and compared it with that in 2D culture (Figure 3 and Supplementary figures S3 and S5). Examination of high-resolution deconvoluted images for EGFP-53BP1 revealed that almost all EGFP-53BP1 foci in 2D cultures treated with γ-rays were efficiently repaired within 24 h; ~8% of DSBs were not repaired in 3D structures at 24 h after γ-irradiation (Figure 3A and B; Supplementary Figure S5). Further, the kinetics of disappearance of EGFP-53BP1 foci in 3D structures irradiated with γ-rays were slower than in the 2D cultures. Mathematical modeling of the 53BP1 foci dissolution data supported this conclusion. The calculated values for fast- and slow dissolution of 53BP1 foci differed significantly in 2D and 3D cultures (Table 1). After 1 Gy of Fe particles irradiation, not all complex DSBs in 2D and 3D structures were efficiently repaired after 72 h (Figure 3A and C; Supplementary Figure S5). As shown in Figure 3C, the average number of residual EGFP-53BP1 foci was ~40% in 3D structures, whereas it was <20% in 2D culture at 72 h after IR, suggesting that a major fraction of complex DSBs were irreparable in 3D structures. Non-linear dynamic fitting of foci dissolution kinetics showed that the rates of loss of 53BP1 foci produced by Fe particles in 3D structures were different than in 2D culture (Table 1). Approximately 71% of complex DSBs in 3D structures were repaired with slow kinetics, whereas only 20% were repaired slowly in 2D culture. Although a significant proportion of Fe particles-induced complex DSBs were irreparable both in 2D and 3D cultures, the percent of persistent foci was relatively higher in 3D structures.

A majority of the complex DNA DSBs induced by iron particles are irreparable in organotypic 3D cultures

To verify whether the complex DNA DSBs induced by Fe particles were repaired with slower kinetics or were irreparable in organotypic 3D culture, we quantitated the number of EGFP-53BP1 foci in 2D and 3D cultures 5 days following Fe particles exposure. As shown in Figure 4A and B, the number of irreparable complex DNA DSBs differed between 2D and 3D cultures. In 2D cells exposed to 10–100 cGy at 5 days post-irradiation, there were 0.25–1.5 53BP1 foci per cell, less than number of foci observed 30 min after irradiation and higher than the background level (Figure 4C). In 3D structures exposed to 10–100 cGy of Fe irradiation, there were 1–4 persistent 53BP1 foci per cell, ~3–4 times higher than the number of residual foci observed in 2D cultures (Figure 4C). Further, when we compared the percentage of residual EGFP-53BP1 in 2D and 3D cultures at 5 days after Fe particles irradiation with that of initially induced foci (at 30 min post-IR), we found that the percent of residual EGFP-53BP1 foci was not non-linear with dose (Supplementary Figure S6). This could be due to the bystander effect. Importantly, the level of residual EGFP-53BP1 foci in 3D structures (ranged between 34% and 48%) was three times higher than that in the 2D cultures (ranged between 10% and 15%). Furthermore, presence of residual EGFP-53BP1 foci did not represent an artifactual response to IR that is unrelated to DSBs as demonstrated by immunostaining both 2D and 3D structures with γH2AX and Chk2 phospho-specific (pT68) antibodies. Chk2 kinase becomes rapidly phosphorylated at threonine 68 (pT68) by ataxia telangiectasia mutated and its activity is limited to sites of DSBs in response to IR (28). As shown in Figure 4A and B, the majority of the EGFP-53BP1 foci clearly colocalized with the phospho-Chk2 and γH2AX foci in irradiated samples, indicating that the 53BP1 foci mark sites of persistent complex DNA DSBs. Thus, the level of irreparable complex DNA DSBs in 3D structures exposed to Fe particles irradiation was relatively higher than that of 2D culture.

Cells containing irreparable DNA DSBs generated by iron particles in 3D structures are differentiated

The elevated levels of irreparable complex DNA DSBs in organotypic 3D culture relative to cells in 2D culture may be due to either the differentiated status of cells in the organotypic culture or the altered expression of multiple DNA repair genes. Evidence suggests that terminally differentiated cells have a reduced capacity to repair DNA lesions (13); therefore, we carefully examined the nature of cells that contained persistent DSBs using a combination of immunostaining and 3D imaging. As shown in Figure 4D, a majority (~95%) of the cells containing persistent EGFP-53BP1 foci were negative for anti-Ki-67 antibody staining at Day 5 following Fe particles irradiation. We also observed a negative correlation between the cells with persistent EGFP-53BP1 foci and Ki-67 staining following 10, 25, 50 and 75 cGy of Fe particles irradiation (data not shown). Conversely, almost all cells with persistent EGFP-53BP1 foci in 2D cultures were positive for Ki-67 staining (Supplementary Figure S4). Thus, virtually all persistent complex DNA DSBs in 3D structures were found in the differentiated cells.

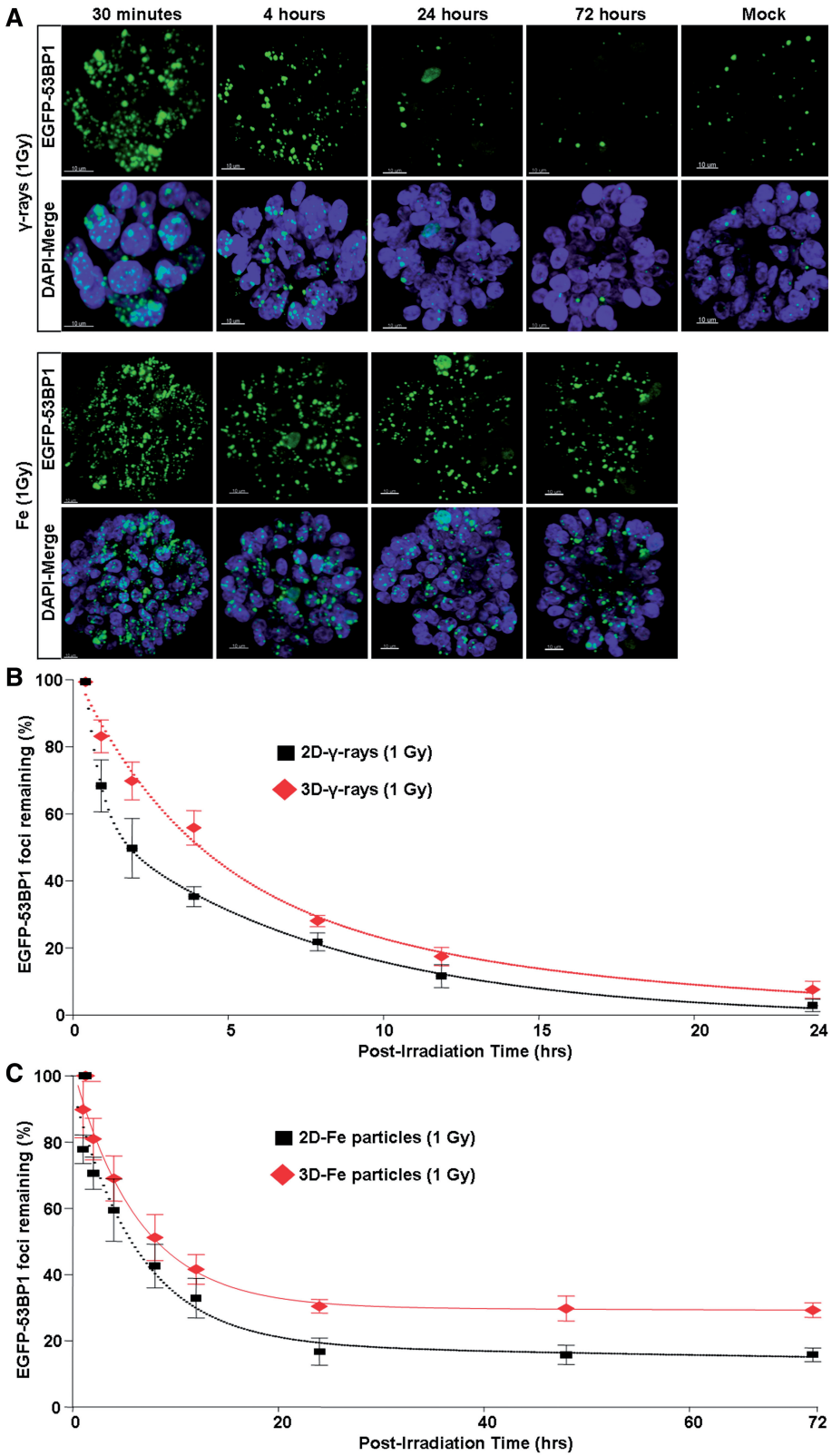

Figure 3. Ionizing radiation-induced DSBs are repaired with slower kinetics in 3D structures than in cells in 2D culture. (**A**) Representative deconvoluted images of 3D structures showing EGFP-53BP1 foci at indicated times after 1 Gy of γ-rays and Fe particles irradiation. HBECs stably expressing EGFP-53BP1 grown in Matrigel for 6 days were irradiated with 1 Gy of γ-rays and Fe particles and were fixed at indicated times after irradiation. Subsequently, images were recorded using confocal microscopy. (**B**) EGFP-53BP1 foci dissolution kinetics are slower in 3D than 2D cultures after 1 Gy of γ-rays or (**C**) Fe particles irradiation. HBECs stably expressing EGFP-53BP1 grown either in 2D or Matrigel, irradiated with 1 Gy of γ-rays and Fe particles and fixed at indicated times. Subsequently, images were acquired using confocal microscopy and the EGFP-53BP1 foci numbers were counted using spot-detection function of Imaris software. The number of EGFP-53BP1 foci in the mock-irradiated cells was subtracted and data were plotted by taking the number of foci at the 30 min time point as 100%. The EGFP-53BP1 foci in 150–200 cells from 2D culture and 15–18 3D structures were counted for each time point. The error bars represent standard deviations calculated from three independent experiments.

Table 1. Non-linear regression-dynamic fitting of EGFP-53BP1 foci dissolution kinetics

Ionizing radiation	Type of culture	Coefficients		SE	R	F slow (%)	F fast (%)
γ-rays	Monolayer	a	118.51	10.58	1.00	34.42	65.58
		b	2.09	0.22			
		c	62.19	2.26			
		d	0.13	0.01			
γ-rays	3D	a	38.40	6.98	1.00	63.73	36.27
		b	0.07	0.08			
		c	67.49	7.29			
		d	0.27	0.20			
Fe particles	Monolayer	a	77.35	11.66	0.99	19.75	80.25
		b	0.16	0.05			
		c	19.03	12.52			
		d	0.00	0.01			
Fe particles	3D	a	29.99	3.68	1.00	70.75	29.25
		b	0.00	0.00			
		c	72.51	3.46			
		d	0.16	0.02			

Equation: $y = ae - bx + ce - dx$,
a and c are the coefficients
a = percentage of foci that are eliminated with fast kinetics
b = rate constant for the fast kinetics
c = percentage of foci that are eliminated with slow kinetics
d = rate constant for the slow kinetics
x = is time (in hours)
F slow = $[c/(a+c)]$
F fast = $[a/(a+c)]$

Downregulation of multiple DNA repair genes results in defective repair of complex DNA DSBs in organotypic 3D culture

The data presented above also suggested that a majority of the DSBs induced by Fe particles, but not the γ-rays, are irreparable in the organotypic culture. DNA lesions induced by Fe particles vary in terms of their overhang configuration and end compatibility; therefore, different repair factors are required to process each DNA lesion type within the complex DNA damage (9). To identify a molecular reason for the inability to repair complex DNA DSBs in 3D culture, we performed a global gene expression analysis using microarrays (Supplementary Figures S7–S10; Table 2, Supplementary Tables S1 and S2). Only 1051 of approximately 48 803 genes reproducibly differed between 2D and 3D mock-treated cultures (Supplementary Figure S7 and Supplementary Table S1). To gain insight into the pathways that were altered in organotypic 3D culture, we conducted gene category enrichment analysis using Ingenuity Pathway Analysis (IPA, Ingenuity® Systems) (20) for multiple DNA repair pathways factors. This analysis revealed that expression of a number of DNA damage response and repair genes was significantly downregulated ($P < 0.01$) in the organotypic 3D culture relative to 2D culture (Supplementary Table S2 and Supplementary Figure S7). Significantly, 212 DNA repair genes reproducibly differed by >1.5-fold between 2D and 3D cultures (Supplementary Table S2). Some of the significant genes expressed at reduced levels in organotypic cultures are presented in Table 2. Furthermore, to determine the biologically relevant networks and pathways of the differentially expressed genes, pathway analysis was done on the up-, down-regulated genes and integrated total datasets using the IPA software. The networks describe functional relationships between gene products based on known interactions reported in the literature. Several significant pathways were recognized in up- and down-regulated genes. All the biological networks that are associated with the DNA repair pathway analyses are presented in the Supplementary Figures S8–S10. Thus, gene expression analyses clearly indicated that defective complex DNA DSB repair in the organotypic 3D cultures was due to the downregulation of multiple DNA repair pathway genes.

Irreparable complex DNA DSBs results in the generation of chromosome aberrations

To determine whether the differences in rejoining kinetics affected the survival of irradiated cells, we examined the ability of cells from monolayer and 3D organotypic cultures to produce colonies after γ- and Fe particles irradiation. In general, cells were more sensitive to Fe particles than to γ-irradiation (Figure 5A). Further, cells derived from 3D structures were more sensitive to γ- and Fe particles irradiation than the cells from 2D culture (Figure 5A). Thus, the differences in DNA lesions rejoining kinetics clearly affected the survival of the irradiated cells. To investigate how impaired DSB repair may lead to the initiation of carcinogenesis, we evaluated chromosomal aberrations in metaphase cells derived from the monolayer and organotypic cultures. Classical chromosome analysis of metaphase spreads revealed that at equal survival dose, the levels of chromosomal aberrations per mitotic cell was higher in both γ-rays and Fe particles-treated 3D structures relative to

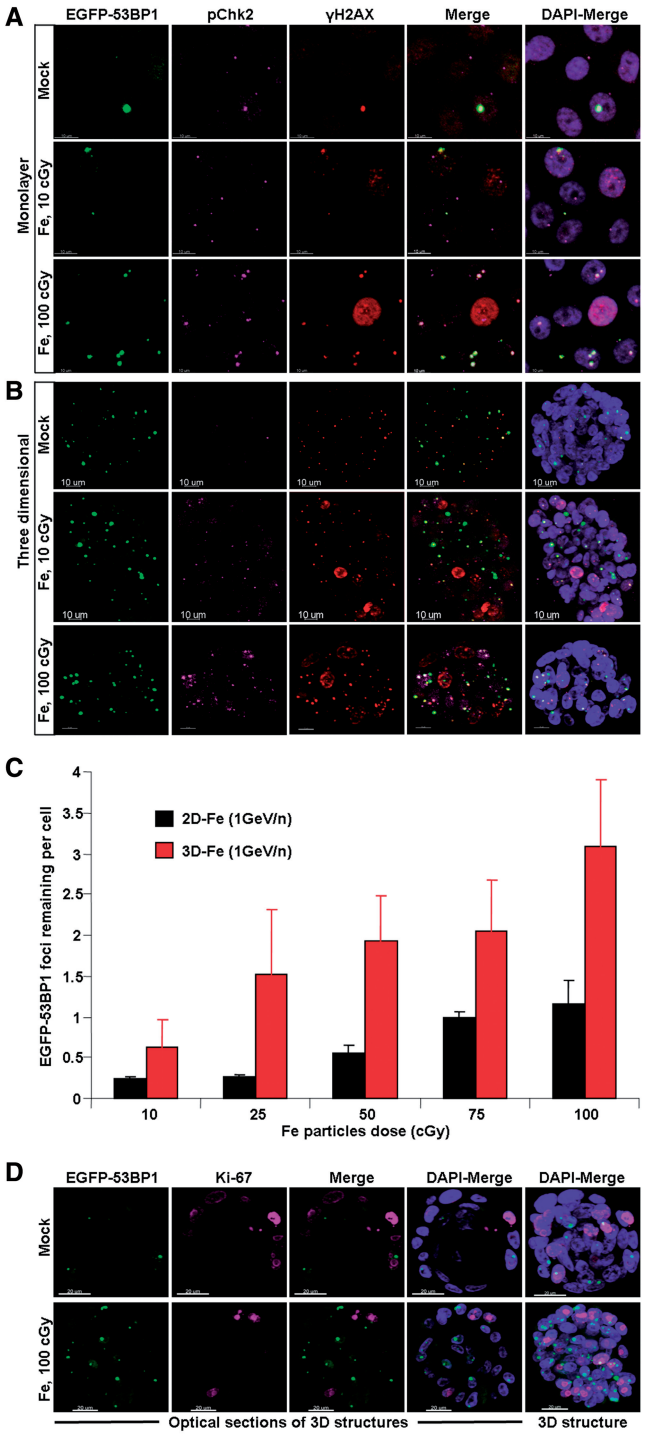

Figure 4. Iron particles-induced complex DSBs persist in 2D and 3D cultures. (**A**) Representative deconvoluted images showing colocalization of persistent EGFP-53BP1 foci with phosphorylated H2AX (γH2AX) and Chk2 (pChk2) in 2D and (**B**) 3D structures. HBECs stably expressing EGFP-53BP1 grown either in 2D or Matrigel, irradiated with indicated doses of Fe particles and were fixed after 5 days. Cells were then immunostained with anti-γH2AX and pChk2 (pT68) antibodies. Images were acquired using confocal microscopy. (**C**) A majority of Fe particles-induced complex DSBs persist in 3D structures. HBECs stably expressing EGFP-53BP1 grown either in 2D or Matrigel, irradiated with indicated doses of Fe particles and fixed after 5 days. Images were acquired using confocal microscopy and the EGFP-53BP1 foci numbers were counted using spot-detection function of the Imaris software. For each dose, the number of EGFP-53BP1 foci in the mock-irradiated cells was subtracted. The EGFP-53BP1 foci in 150–200 cells from 2D culture and 15–18 3D structures were counted for each dose. The error bars represent standard deviations calculated from three independent experiments. (**D**) Cells containing irreparable complex DNA DSBs generated by Fe particles in 3D structures are differentiated. Representative deconvoluted images showing localization of EGFP-53BP1 foci in the differentiated cells (Ki-67 negative) of 3D structures. HBECs stably expressing EGFP-53BP1 were grown in Matrigel for 6 days, exposed to 1 Gy of Fe particles and were fixed at 5 days after irradiation. Subsequently, cells were immunostained with anti-Ki-67 antibodies and the images were acquired using confocal microscopy and deconvoluted using Imaris software.

2D culture (Figure 5B). Interestingly, cells exposed to Fe particles had significantly elevated levels of chromosomal aberrations per mitotic cell relative to levels in γ-irradiated samples (Figure 5B). Specifically, in cells derived from 3D structures the average number of aberrations per cell was approximately 1.4 for Fe particles treated cells and was only approximately 1 aberration per cell for those treated with γ-rays (Figure 5B). On the other hand, in cells derived from 2D cultures, the average number of aberrations per cell was approximately 1.1 for Fe particles-treated cells and was approximately 0.7 aberration per cell for those treated with γ-rays (Figure 5B). Further, both γ- and Fe particles irradiation induced a spectrum of chromatid and chromosomal aberrations both in 2D and 3D cultures and the extent was clearly dependent on the type of DNA lesions (Figure 5C). Detailed analysis of chromatid (breaks, triradials and quadriradials) and chromosome (breaks, dicentrics and rings) aberrations revealed that cells from 3D structures were devoid of triradials, quadriradials and rings (Figure 5C). In contrast, 2D cells displayed all types of aberrations (Figure 5C). Together, these data reveal that cells from 3D structures display higher levels of chromosomal aberrations in response to IR and the number of chromosome aberrations correlates with the number of persistent DSBs induced by high-LET radiation. The genomic instability that results from these aberrations presumably facilitates the initiation of carcinogenesis. Though differentiated cells are not expected to replicate their genomes, unexpected events like tissue damage repair (29) may force cells to re-enter the cell cycle and replicate and transcribe a genome crippled by lesions; this might trigger carcinogenic events.

DISCUSSION

To our knowledge, this article describes for the first time the observation of induction and repair of DNA DSBs induced by IR in a lung organotypic 3D culture model. We first confirmed that HBECs grown in Matrigel on the top of human fetal lung fibroblasts differentiate into peripheral lung-specific structures (25). Second, we confirmed that DSBs induced by γ- or Fe particles irradiation were repaired with slower kinetics in cells grown in organotypic culture than in 2D culture. Our results are in agreement with the notion that DNA repair is attenuated in differentiated cells (13,15,30). Third, although a significant proportion of Fe particles-induced complex DNA DSBs

Table 2. Genes involved in multiple DNA repair pathways that are significantly down-regulated in the organotypic culture as compared with monolayer culture

Gene symbol	Entrez gene name	Fold change
BLM	Bloom syndrome, RecQ helicase like	−5.74
BRCA1	Breast cancer 1, early onset	−6.60
CDC25A	Cell division cycle 25 homolog A (*Schizosaccharomyces pombe*)	−6.43
CDC25C	Cell division cycle 25 homolog C (*S. pombe*)	−9.79
CHEK1	CHK1 checkpoint homolog (*S. pombe*)	−4.47
CHEK2	CHK2 checkpoint homolog (*S. pombe*)	−3.23
ERCC1	Excision repair cross-complementing rodent repair deficiency, complementation Group 1	−5.94
ERCC6L	Excision repair cross-complementing rodent repair deficiency, complementation group 6-like	−9.15
EXO1	Exonuclease 1	−6.60
FEN1	Flap structure-specific endonuclease 1	−5.99
MCM10	Minichromosome maintenance complex component 10	−6.62
NTHL1	nth endonuclease III-like 1 (*Escherichia coli*)	−2.27
PCNA	Proliferating cell nuclear antigen	−2.27
PLK1	Polo-like kinase 1 (*Drosophila*)	−5.90
PNKP	Polynucleotide kinase 3′-phosphatase	−2.20
RAD51	RAD51 homolog (RecA homolog, *E. coli*) (*Saccharomyces cerevisiae*)	−3.67
RAD51L1	RAD51-like 1 (*S. cerevisiae*)	−3.71
RAD54B	RAD54 homolog B (*S. cerevisiae*)	−2.37
RAD54L	RAD54-like (*S. cerevisiae*)	−3.80
RECQL	RecQ protein-like (DNA helicase Q1-like)	−2.28
RECQL4	RecQ protein-like 4	−4.48
SMC2	Structural maintenance of chromosomes 2	−3.84
SMC4	Structural maintenance of chromosomes 4	−9.99
XRCC3	X-ray repair complementing defective repair in Chinese hamster cells 3	−5.52

were irreparable both in 2D and 3D structures, the number of persistent DNA lesions was higher in 3D structures. These data support the idea that the difficulties associated with the repair of complex DSBs are due to the nature of the complex clustered DNA damage induced by dense ionizations (31). Fourth, we provided molecular evidence that the defective complex DSB repair was due to the downregulation of multiple DNA repair pathway genes in organotypic 3D culture. Finally, upon resumption of the cell cycle, differentiated cells with unrepaired DSBs manifested a spectrum of chromosomal aberrations in mitosis. Thus, our data suggest that downregulation of multiple DNA repair pathway genes in differentiated cells renders them vulnerable to chromosomal damage and may promote genome instability leading to carcinogenesis.

Our data on DSBs repair kinetics revealed that a major proportion of DSBs persisted both in 2D and 3D cultures following high-LET IR; DSBs did not persist to this extent following γ-irradiation. Other studies have also reported the presence of unrepaired DNA damage after exposure of monolayer cultures to high-LET radiation (9,22,32,33). DNA lesions induced by γ-rays, including DSBs, SSBs and damaged bases are usually located at a distance from other damages and are generally repaired efficiently (7). High-LET radiation induces complex DNA damage (34). Convincing evidence indicates that clustered DNA damage is more difficult for the cellular machinery to repair than are individual damage sites. Studies with synthetic oligonucleotides containing several types of DNA damage have shown that the efficiency of incision of an AP site, for example, within a region of clustered DNA damage is significantly reduced by the presence of a second AP site or SSB (35). Similarly, APs or 8-oxoguanine (8-OxoG) sites within clustered DNA damage sites are poorly handled by mammalian cell extracts or purified repair enzymes (36–38). These unrepaired cluster DNA lesions may generate additional DSBs (32,39). Clustered DNA damage sites appear to retard the function of repair enzymes. Theoretical modeling to simulate the dynamics of clustered DNA damage sites containing abasic or 8-OxoG sites suggest that these lesions cause DNA to adopt non-canonical conformations (40). These conformations may make it difficult for repair enzymes to bind to the region, thereby resulting in a reduction of repair efficiency. Further, model system studies of oligonucleotides and plasmids with defined lesions at specific spacings on opposing strands indicate that clusters may comprise non-repairable, highly repair-resistant, or pre-mutagenic damage (6,39,41–43).

Although the initial number of 53BP1 foci measured at 30 min after Fe particles irradiation increased with increasing Fe particles dose from 10 to 100 cGy, the percent of residual 53BP1 foci measured at 5 days after IR was not linear in either 2D or 3D structures. This could be due to the bystander effect. Further, unlike the induction of initial number of EGFP-53BP1 foci in 2D cultures, it is likely that the contribution of the bystander effect to the residual number of EGFP-53BP1 foci at 5 days after IR would be higher at later time points than earlier, due to the differences in cell density. As suggested in a previous report (44), it is possible that the irreparable DNA lesions in the irradiated cells continuously release DNA damaging agents to the bystander cells resulting in DSBs. Masking of the

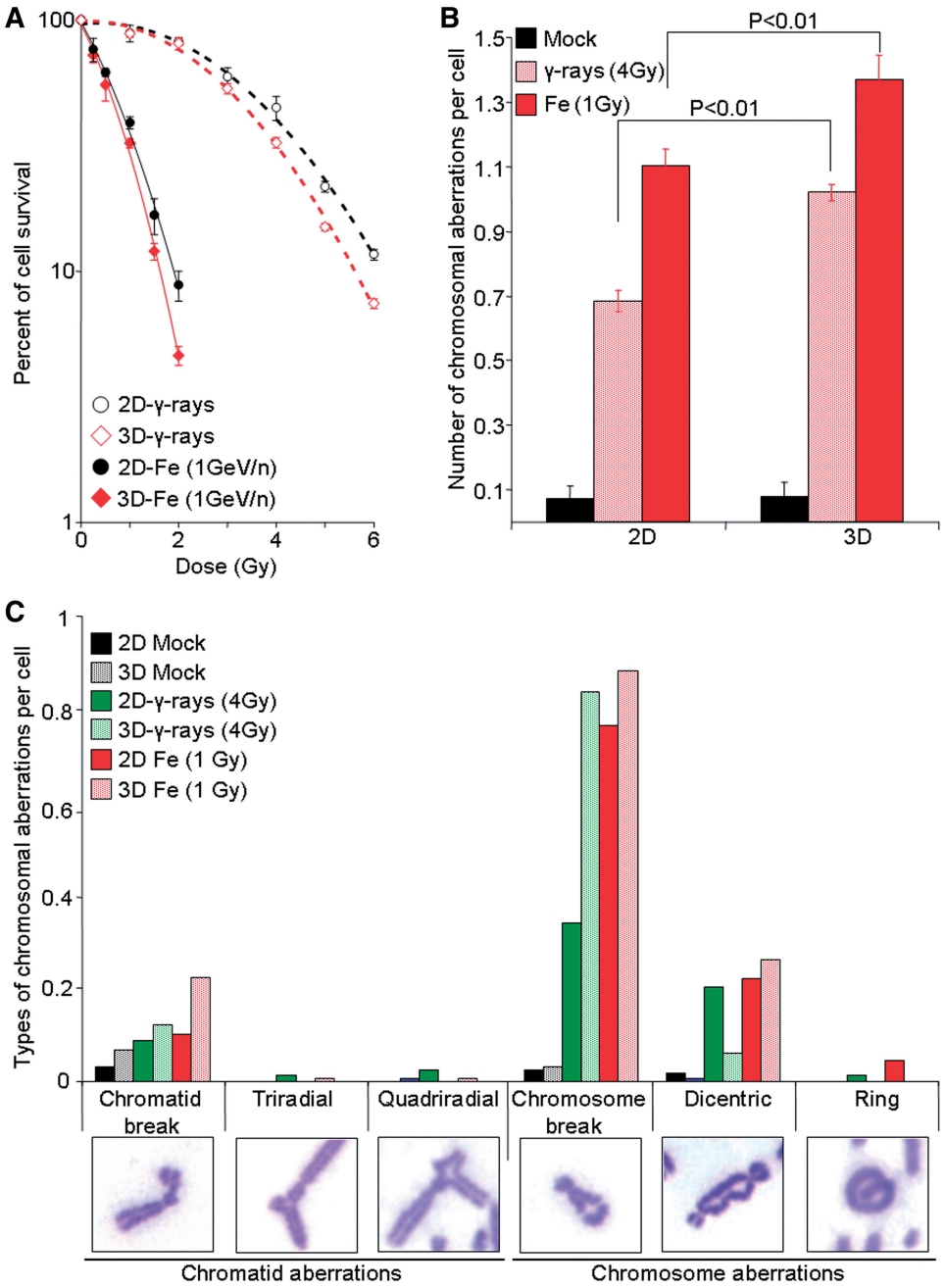

Figure 5. Irreparable complex DSB repair leads to the generation of chromosome aberrations. (**A**) Iron particles-induced cell killing is greater than that for γ-rays. HBECs grown in 3D and 2D cultures were irradiated with graded doses of γ-rays and Fe particles. After 4 h, the 3D structures were dissociated. Cells from the 3D structures and 2D cultures were subjected to a colony formation assay. Each data point is the mean and standard deviations from at least two 3D or three 2D independent experiments. (**B**) The number of chromosomal aberrations induced by γ-rays and Fe particles are higher in cells derived from 3D culture. (**C**) Cells derived from 3D structures display distinct types of gross chromosomal aberrations. The 3D structures and 2D culture were irradiated with indicated doses of γ-rays or Fe particles. The 3D structures were dissociated from the Matrigel 24 h following IR and then cultured for an additional 24 h. Subsequently, chromosome preparations were made by accumulating metaphases in the presence of 0.1 μg/ml colcemid for 8 h. For each radiation type, more than 100 metaphase spreads were prepared. Each data point in the graph is the average of two or three independent experiments.

bystander effect at higher doses might be the reason why the residual 53BP1 foci measured at 5 days after IR was not linear in either 2D or 3D cultures. Additional work is needed to determine whether all the persistent DNA lesions in the bystander cells are complex DSBs. Importantly, disappearance of majority of 53BP1 foci in 2D cultures, not the 3D cultures, by 5 days after Fe particles irradiation indicates that the cells in 2D cultures were capable of repairing the DNA damage but that cells in 3D structures were not.

Although a major proportion of Fe particles-induced complex DNA DSBs were irreparable both in 2D (10–15%) and 3D (34–48%) cultures, the number of persistent DNA lesions was higher in 3D structures. We

envisaged two scenarios that might hamper the ability of cells in organotypic culture to repair complex DNA DSBs: the cell cycle distribution and the differentiated status of the cells. IR-induced DSBs are repaired via two mechanistically distinct pathways: homologous recombination (HR) and non-homologous end-joining (NHEJ). HR is a high-fidelity repair mechanism that occurs preferentially during the late S- and G2-phases of the cell cycle when a sister chromatid is present and therefore this pathway is precluded in non-cycling cells. NHEJ simply pieces together the broken DNA ends and functions in all phases of the cell cycle (45,46). In proliferating cells, the Ku-dependent NHEJ is not necessary for high-LET radiation-induced DSB repair (47). We hypothesize that due to the large numbers of G0-phase (or differentiated) cells in 3D culture, Fe particles-induced DSBs may not be repaired via NHEJ pathway. However, when we irradiated growth-arrested 2D cultures with Fe particles, the number of residual DSBs at Day 5 was similar to that observed in exponentially growing cells (data not shown), suggesting that the difficulties associated with the repair of complex DNA DSBs in organotypic culture are not associated with the cell cycle distribution. Evidence suggests that terminally differentiated cells have a reduced capacity to repair DNA lesions (13,15,30,48). Immunostaining for Ki-67 in a 3D imaging approach revealed that the majority of the persistent DNA lesions were found in differentiated cells, indicating that the difficulties associated with the repair of complex DNA lesions in organotypic culture are due to the differentiated stage of the cells. It has been shown that in differentiated K562 cells there is a retarded rejoining of DNA breaks (48) and in several differentiated cell systems DNA repair is attenuated at the global level, but maintained in expressed genes (13). Collectively, these data confirm that differentiated cells are defective in complex DNA lesion repair.

What is the molecular mechanism for the defective complex DSB repair in 3D organotypic culture? Our data on the ingenuity pathway analysis of global gene expression profile indicated that expression of genes that have been shown to facilitate multiple DNA repair pathways were significantly down-regulated in the organotypic culture as compared with 2D culture. Some specific DSB repair proteins, such as Chek1, Ku, H2AX (15) and BRCA1 (49) are known to be down-regulated in terminally differentiated cells. In addition, other repair pathways, such as base excision repair, have diminished activity after terminal differentiation (50). DNA lesions induced by high-LET radiation may vary in terms of their overhang configuration and end compatibility; therefore various repair factors are required to process each specific DNA lesion type within the complex DNA damage (9). Thus, our results imply that the down-regulation of multiple DNA repair pathway genes in differentiated human lung epithelial cells is the molecular reason for the defective complex DNA lesions repair.

Differentiated cells do not usually replicate their genomes and may dispense with the burden of repairing the bulk of their genomic DNA, as long as the integrity of actively expressed genes is maintained. This parsimonious strategy may backfire, though, if unexpected events—like tissue damage—force cells to re-enter the cell cycle and replicate a genome crippled by lesions (13). Our classical chromosome analysis of metaphase spreads derived from organotypic cultures that were forced to re-enter the cell cycle revealed that in cells exposed to γ-irradiation or to Fe particles the levels of chromosomal aberrations per mitotic cell were significantly elevated relative to cells in 2D culture. The levels of chromosomal abnormalities were clearly correlated with the nature of the DNA damage in organotypic culture. Presence of high-level of chromosome aberrations in Fe particles irradiated samples, can be explained by the fact that the non-repairable DSB clusters accumulating at high levels in 3D cultures treated with Fe particles, through DNA replication in S-phase and chromatin condensation during G2- to M-phase transition were expected to be converted and visualized at metaphase mainly as chromosome breaks. Furthermore, if chromatid breaks occur at two adjacent sites on two different chromosomes, asymmetrical or symmetrical quadriradial chromosomes could be formed depending on the way of rejoining. For instance, in the following mitosis, asymmetrical quadriradials derive unstable chromosome-type aberrations (e.g. dicentrics and acentric fragments) and symmetrical quadriradials derive stable aberrations (e.g. reciprocal translocations) (51). In addition, our cell survival data revealed that the differences in clustered DNA lesions rejoining kinetics clearly affected the survival of the irradiated cells. Although most irradiated cells die due to their inability to complete mitosis, some cells with repair-resistant DNA lesions survive and enter into mitosis. Every round of replication is expected to increase the overall mutation level and lead to accumulation of mutations in surviving cells (52). Therefore, we believe that the biological significance of HZE particles induced damage is high in differentiated cells, since unexpected events—like tissue damage—force cells to re-enter the cell cycle and replicate a genome crippled by lesions can provide the opportunity for genomic rearrangements and can increase genomic instability leading to genetic changes required for progression from an initiated cell to a metastatic tumor cell.

In summary, this is the first comprehensive study to demonstrate the biological impact of defective DNA DSB repair in differentiated lung epithelial cells. Using a 3D human lung epithelial cell system, we confirmed that DNA repair is attenuated in differentiated cells. Further, we provided evidence that repair of the complex DSBs induced by high-LET Fe particles but not the isolated DSBs induced by γ-rays was substantially compromised in differentiated human lung epithelial cells compared to proliferating cultures of the same cells. We provided molecular evidence that the difficulties associated with complex DNA lesion repair in organotypic culture was due to the down-regulation of multiple DNA repair pathway genes. Significantly, upon resumption of cell cycle, differentiated cells with unrepaired DSBs manifested a spectrum of chromosomal aberrations in mitosis. If unexpected events force these cells to replicate, the unrepaired lesions might trigger carcinogenic events. As the organotypic 3D model mimics human lung, it

opens up new experimental approaches to explore the effect of radiation *in vivo* and will have important implications for evaluating radiation risk on human lung carcinogenesis and cancer therapy.

SUPPLEMENTARY DATA

Supplementary Data are available at NAR Online.

ACKNOWLEDGEMENTS

We thank Peter Guida, Adam Rusek and Angela Kim of Brookhaven National Laboratory for their help in iron particles irradiation.

FUNDING

National Aeronautics and Space Administration [NNZ07AU42G to D.J.C.]; National Aeronautics and Space Administration Specialized Center of Research [NNX11AC54G to J.D.M.]; and the National Institutes of Health [CA134991 to D.J.C.]. Funding for open access charge: National Aeronautics and Space Administration Specialized Center of Research.

Conflict of interest statement. None declared.

REFERENCES

1. Nikjoo,H., O'Neill,P., Wilson,W.E. and Goodhead,D.T. (2001) Computational approach for determining the spectrum of DNA damage induced by ionizing radiation. *Radiat. Res.*, **156**, 577–583.
2. Goodhead,D.T. (1994) Initial events in the cellular effects of ionizing radiations: clustered damage in DNA. *Int. J. Radiat. Biol.*, **65**, 7–17.
3. Ward,J.F. (1988) DNA damage produced by ionizing radiation in mammalian cells: identities, mechanisms of formation, and reparability. *Prog. Nucleic Acid Res. Mol. Biol.*, **35**, 95–125.
4. Brenner,D.J. and Ward,J.F. (1992) Constraints on energy deposition and target size of multiply damaged sites associated with DNA double-strand breaks. *Int. J. Radiat. Biol.*, **61**, 737–748.
5. Blaisdell,J.O., Harrison,L. and Wallace,S.S. (2001) Base excision repair processing of radiation-induced clustered DNA lesions. *Radiat. Prot. Dosimetry*, **97**, 25–31.
6. Harrison,L., Hatahet,Z., Purmal,A.A. and Wallace,S.S. (1998) Multiply damaged sites in DNA: interactions with Escherichia coli endonucleases III and VIII. *Nucleic Acids Res.*, **26**, 932–941.
7. Sutherland,B.M., Bennett,P.V., Sidorkina,O. and Laval,J. (2000) Clustered DNA damages induced in isolated DNA and in human cells by low doses of ionizing radiation. *Proc. Natl Acad. Sci. USA*, **97**, 103–108.
8. Kramer,M., Weyrather,W.K. and Scholz,M. (2003) The increased biological effectiveness of heavy charged particles: from radiobiology to treatment planning. *Technol. Cancer Res. Treat.*, **2**, 427–436.
9. Asaithamby,A. and Chen,D.J. (2010) Mechanism of cluster DNA damage repair in response to high-atomic number and energy particles radiation. *Mutat. Res.*, doi:10.1016/j.mrfmmm.2010.11.002.
10. Weigelt,B. and Bissell,M.J. (2008) Unraveling the microenvironmental influences on the normal mammary gland and breast cancer. *Semin. Cancer Biol.*, **18**, 311–321.
11. Rhee,S. and Grinnell,F. (2007) Fibroblast mechanics in 3D collagen matrices. *Adv. Drug Deliv. Rev.*, **59**, 1299–1305.
12. Emerman,J.T. and Pitelka,D.R. (1977) Maintenance and induction of morphological differentiation in dissociated mammary epithelium on floating collagen membranes. *In Vitro*, **13**, 316–328.
13. Nouspikel,T. (2007) DNA repair in differentiated cells: some new answers to old questions. *Neuroscience*, **145**, 1213–1221.
14. Harper,J.V., Anderson,J.A. and O'Neill,P. (2010) Radiation induced DNA DSBs: Contribution from stalled replication forks? *DNA Repair*, **9**, 907–913.
15. Lal,A., Pan,Y., Navarro,F., Dykxhoorn,D.M., Moreau,L., Meire,E., Bentwich,Z., Lieberman,J. and Chowdhury,D. (2009) miR-24-mediated downregulation of H2AX suppresses DNA repair in terminally differentiated blood cells. *Nat. Struct. Mol. Biol.*, **16**, 492–498.
16. Ramirez,R.D., Sheridan,S., Girard,L., Sato,M., Kim,Y., Pollack,J., Peyton,M., Zou,Y., Kurie,J.M., Dimaio,J.M. *et al.* (2004) Immortalization of human bronchial epithelial cells in the absence of viral oncoproteins. *Cancer Res.*, **64**, 9027–9034.
17. Asaithamby,A. and Chen,D.J. (2009) Cellular responses to DNA double-strand breaks after low-dose gamma-irradiation. *Nucleic Acids Res.*, **37**, 3912–3923.
18. Lee,G.Y., Kenny,P.A., Lee,E.H. and Bissell,M.J. (2007) Three-dimensional culture models of normal and malignant breast epithelial cells. *Nat. Methods*, **4**, 359–365.
19. Chen,B.P., Chan,D.W., Kobayashi,J., Burma,S., Asaithamby,A., Morotomi-Yano,K., Botvinick,E., Qin,J. and Chen,D.J. (2005) Cell cycle dependence of DNA-dependent protein kinase phosphorylation in response to DNA double strand breaks. *J. Biol. Chem.*, **280**, 14709–14715.
20. Ding,L.H., Xie,Y., Park,S., Xiao,G. and Story,M.D. (2008) Enhanced identification and biological validation of differential gene expression via Illumina whole-genome expression arrays through the use of the model-based background correction methodology. *Nucleic Acids Res.*, **36**, e58.
21. DiBiase,S.J., Zeng,Z.C., Chen,R., Hyslop,T., Curran,W.J. Jr and Iliakis,G. (2000) DNA-dependent protein kinase stimulates an independently active, nonhomologous, end-joining apparatus. *Cancer Res.*, **60**, 1245–1253.
22. Asaithamby,A., Uematsu,N., Chatterjee,A., Story,M.D., Burma,S. and Chen,D.J. (2008) Repair of HZE-particle-induced DNA double-strand breaks in normal human fibroblasts. *Radiat. Res.*, **169**, 437–446.
23. Van Haute,L., De Block,G., Liebaers,I., Sermon,K. and De Rycke,M. (2009) Generation of lung epithelial-like tissue from human embryonic stem cells. *Respir. Res.*, **10**, 105.
24. Gerdes,J., Lemke,H., Baisch,H., Wacker,H.H., Schwab,U. and Stein,H. (1984) Cell cycle analysis of a cell proliferation-associated human nuclear antigen defined by the monoclonal antibody Ki-67. *J. Immunol.*, **133**, 1710–1715.
25. Vaughan,M.B., Ramirez,R.D., Wright,W.E., Minna,J.D. and Shay,J.W. (2006) A three-dimensional model of differentiation of immortalized human bronchial epithelial cells. *Differentiation*, **74**, 141–148.
26. Su,Y., Meador,J.A., Geard,C.R. and Balajee,A.S. (2010) Analysis of ionizing radiation-induced DNA damage and repair in three-dimensional human skin model system. *Exp. Dermatol.*, **19**, e16–22.
27. Schultz,L.B., Chehab,N.H., Malikzay,A. and Halazonetis,T.D. (2000) p53 binding protein 1 (53BP1) is an early participant in the cellular response to DNA double-strand breaks. *J. Cell Biol.*, **151**, 1381–1390.
28. Ward,I.M., Wu,X. and Chen,J. (2001) Threonine 68 of Chk2 is phosphorylated at sites of DNA strand breaks. *J. Biol. Chem.*, **276**, 47755–47758.
29. Crosby,L.M. and Waters,C.M. (2010) Epithelial repair mechanisms in the lung. *Am. J. Physiol. Lung Cell Mol. Physiol.*, **298**, L715–731.
30. Fortini,P. and Dogliotti,E. (2010) Mechanisms of dealing with DNA damage in terminally differentiated cells. *Mutat. Res.*, **685**, 38–44.
31. Goodhead,D.T. (2006) Energy deposition stochastics and track structure: what about the target? *Radiat. Prot. Dosimetry*, **122**, 3–15.

32. Gulston,M., de Lara,C., Jenner,T., Davis,E. and O'Neill,P. (2004) Processing of clustered DNA damage generates additional double-strand breaks in mammalian cells post-irradiation. *Nucleic Acids Res.*, **32**, 1602–1609.
33. Desai,N., Davis,E., O'Neill,P., Durante,M., Cucinotta,F.A. and Wu,H. (2005) Immunofluorescence detection of clustered gamma-H2AX foci induced by HZE-particle radiation. *Radiat. Res.*, **164**, 518–522.
34. Hada,M. and Georgakilas,A.G. (2008) Formation of clustered DNA damage after high-LET irradiation: a review. *J. Radiat. Res.*, **49**, 203–210.
35. David-Cordonnier,M.H., Cunniffe,S.M., Hickson,I.D. and O'Neill,P. (2002) Efficiency of incision of an AP site within clustered DNA damage by the major human AP endonuclease. *Biochemistry*, **41**, 634–642.
36. Gulston,M., Fulford,J., Jenner,T., de Lara,C. and O'Neill,P. (2002) Clustered DNA damage induced by gamma radiation in human fibroblasts (HF19), hamster (V79-4) cells and plasmid DNA is revealed as Fpg and Nth sensitive sites. *Nucleic Acids Res.*, **30**, 3464–3472.
37. Budworth,H., Dianova,I.I., Podust,V.N. and Dianov,G.L. (2002) Repair of clustered DNA lesions. Sequence-specific inhibition of long-patch base excision repair be 8-oxoguanine. *J. Biol. Chem.*, **277**, 21300–21305.
38. Lomax,M.E., Cunniffe,S. and O'Neill,P. (2004) Efficiency of repair of an abasic site within DNA clustered damage sites by mammalian cell nuclear extracts. *Biochemistry*, **43**, 11017–11026.
39. Eccles,L.J., Lomax,M.E. and O'Neill,P. (2010) Hierarchy of lesion processing governs the repair, double-strand break formation and mutability of three-lesion clustered DNA damage. *Nucleic Acids Res.*, **38**, 1123–1134.
40. Fujimoto,H., Pinak,M., Nemoto,T., O'Neill,P., Kume,E., Saito,K. and Maekawa,H. (2005) Molecular dynamics simulation of clustered DNA damage sites containing 8-oxoguanine and abasic site. *J. Comput. Chem.*, **26**, 788–798.
41. Harrison,L., Hatahet,Z. and Wallace,S.S. (1999) In vitro repair of synthetic ionizing radiation-induced multiply damaged DNA sites. *J. Mol. Biol.*, **290**, 667–684.
42. Malyarchuk,S., Castore,R. and Harrison,L. (2008) DNA repair of clustered lesions in mammalian cells: involvement of non-homologous end-joining. *Nucleic Acids Res.*, **36**, 4872–4882.
43. Bellon,S., Shikazono,N., Cunniffe,S., Lomax,M. and O'Neill,P. (2009) Processing of thymine glycol in a clustered DNA damage site: mutagenic or cytotoxic. *Nucleic Acids Res.*, **37**, 4430–4440.
44. Sedelnikova,O.A., Nakamura,A., Kovalchuk,O., Koturbash,I., Mitchell,S.A., Marino,S.A., Brenner,D.J. and Bonner,W.M. (2007) DNA double-strand breaks form in bystander cells after microbeam irradiation of three-dimensional human tissue models. *Cancer Res.*, **67**, 4295–4302.
45. Rothkamm,K., Kruger,I., Thompson,L.H. and Lobrich,M. (2003) Pathways of DNA double-strand break repair during the mammalian cell cycle. *Mol. Cell. Biol.*, **23**, 5706–5715.
46. Lieber,M.R. (2010) The mechanism of double-strand DNA break repair by the nonhomologous DNA end-joining pathway. *Annu. Rev. Biochem.*, **79**, 181–211.
47. Wang,H., Zhang,X., Wang,P., Yu,X., Essers,J., Chen,D., Kanaar,R., Takeda,S. and Wang,Y. (2010) Characteristics of DNA-binding proteins determine the biological sensitivity to high-linear energy transfer radiation. *Nucleic Acids Res.*, **38**, 3245–3251.
48. Tabocchini,M.A., Rothkamm,K., Signoretti,C., Risse,J., Sapora,O. and Lobrich,M. (2000) Formation and repair of DNA double-strand breaks in gamma-irradiated K562 cells undergoing erythroid differentiation. *Mutat. Res.*, **461**, 71–82.
49. Moskwa,P., Buffa,F.M., Pan,Y., Panchakshari,R., Gottipati,P., Muschel,R.J., Beech,J., Kulshrestha,R., Abdelmohsen,K., Weinstock,D.M. *et al.* (2011) miR-182-mediated downregulation of BRCA1 impacts DNA repair and sensitivity to PARP inhibitors. *Mol. Cell*, **41**, 210–220.
50. Narciso,L., Fortini,P., Pajalunga,D., Franchitto,A., Liu,P., Degan,P., Frechet,M., Demple,B., Crescenzi,M. and Dogliotti,E. (2007) Terminally differentiated muscle cells are defective in base excision DNA repair and hypersensitive to oxygen injury. *Proc. Natl Acad. Sci. USA*, **104**, 17010–17015.
51. Satoh,T., Hatanaka,M., Yamamoto,K., Kuro-o,M. and Sofuni,T. (2002) Application of mFISH for the analysis of chemically-induced chromosomal aberrations: a model for the formation of triradial chromosomes. *Mutat. Res.*, **504**, 57–65.
52. Holt,S.M., Scemama,J.L., Panayiotidis,M.I. and Georgakilas,A.G. (2009) Compromised repair of clustered DNA damage in the human acute lymphoblastic leukemia MSH2-deficient NALM-6 cells. *Mutat. Res.*, **674**, 123–130.